BIOMIMETIC-INSPIRED COMPOSITE TO METAL SINGLE LAP JOINTS

E. I. Avgoulas[a*], M. P. F. Sutcliffe[a]

[a]*Department of Engineering, University of Cambridge, Trumpington Street, Cambridge, CB2 1PZ United Kingdom*
**eia21@cam.ac.uk*

Keywords: Adhesive SLJs, composite, metal, biomimetics.

Abstract
Joining composites with metal parts leads, inevitably, to high stress concentrations because of the material property mismatch. Since joining composite to metal is required in many high performance structures, there is a need to develop a new multifunctional approach to meet this challenge. This paper uses the biomimetics approach to help develop solutions to this problem. Nature has found many ingenious ways of joining dissimilar materials and making robust attachments, alleviating potential stress concentrations. One of the key characteristics that nature uses to joint dissimilar materials is a transitional zone of stiffness in the insertion site. Several biomimetic-inspired metal-to-composite (steel-to-CFRP), adhesively bonded, Single Lap Joints (SLJs) were numerically investigated using a finite element analysis. The proposed solutions offer a transitional zone of stiffness of one joint part to reduce the material stiffness mismatch at the joint. An optimisation procedure was used to identify the variation in material stiffness which minimises potential failure of the joint. It was found that the proposed biomimetic SLJs reduce the asymmetry of the stress distribution along the adhesive area, giving a 59% shear stress reduction in some configurations.

1. Introduction

Joining, together with damage tolerance and inserts, are of paramount importance in mechanical design because they cause structural discontinuities that are often the Achilles heel of a structural design. It would be ideal for the design engineers to make structures without joints, eliminating sources of complexity and weakness, as well as reducing weight. Undoubtedly, this ideal can never be realised due to many reasons, such as requirements for structure disassembly due to transportation, access for repair and inspection, size limitations imposed by the materials or manufacture processes, etc. Some of the difficulties with joining dissimilar materials, such as CFRP and steel, are related to the large difference in material properties (e.g. stiffness, coefficient of thermal expansion, etc.) between the adherends. The stiffness mismatch leads to high stress concentrations, and accordingly weak joints [1]. Therefore, there is the need for a new multifunctional joining method that will lead to the next generation of joining technologies.

But who can inspire researchers and engineers in order to find a new joint method? The answer is simple: nature. Nature has a huge advantage comparing with any human-being research team: plenty of time, and actually 3.8 billions of years of research and development

programme. Throughout these years nature has produced amazing designs that engineers have not yet found a way to simulate in man-made structures. A biomimetic-inspired approach to find a new innovative joint method sounds attractive.

In the present study, the idea of a transitional zone of stiffness used by natural joint designs [2] was adapted to adhesively bonded SLJs. The aim is to evaluate the hypothesis that the asymmetry of the stress concentration at the ends of the overlap length of steel-to-CFRP SLJs, caused by the material property mismatch, can be reduced using this biomimetic-inspired design strategy.

2. Finite element modeling

2.1. Numerical modeling

Several biomimetic-inspired metal-to-composite, adhesively bonded, Single Lap Joints (SLJs) were numerically investigated using the Finite Element Analysis (FEA) software ABAQUS, see the overall configuration sketch in Fig. 1.

The thickness of the adherends and the adhesive was 5.5 mm and 0.1 mm, respectively. An Overlap Length (OL) of 75 mm was used. Biquadratic 8-node quadrilateral elements (CPS8R) available in the ABAQUS element library were used for both adherends and adhesive. Mesh refinement studies were carried out to choose the mesh density. Fixed boundary conditions were applied to the CFRP end of the joint and a concentrated force of 15 kN was applied to the steel end of the model.

2.2. Configurations investigated

The configurations investigated included reference joints, where there is no change in stiffness within each part (i.e. metal or CFRP) of the joint. For this "REF" configuration, the unidirectional CFRP adherends were modelled as a linear elastic material with Young modulus (stiffness) in the principal axis 1 (the loading direction) E_{1C} = 100 GPa. The steel adherends were modelled as an isotropic linear elastic material with stiffness E_S = 200 GPa and Poisson ratio equals to 0.28.

On the other hand, the proposed solutions included a transitional zone of stiffness in the overlap region of the metal part to reduce the material stiffness mismatch at the joint site (see Figure 1). An optimisation procedure was used to identify the variation in material stiffness which minimises potential failure of the joint. Different sets of variable stiffness functions were used to optimise the material stiffness variation, identifying for each set the best stiffness function. A complete list of the configurations under investigation is presented in Table 1.

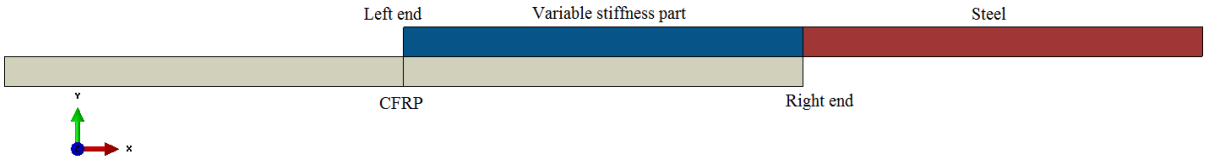

Figure 1. Coordinate system and materials of the SLJ.

The stiffness $E(x)$ of the metal part as a function of the position x along the OL of the joint was varied from 200 to 100 GPa using parabolic (see Test 1, Table 1) and s-shaped functions (see Test 12, Table 1) as defined by equations (1) and (2), respectively;

$$E(x)=100+100\left(\frac{x}{x_c}\right)^b \tag{1}$$

and

$$E(x)=100+\frac{100}{1+e^{-ax}} \tag{2}$$

where, $E(x)$ is in GPa and x_c is the overlap length. The parameters a and b defining the shape of the curves were spaced logarithmically. Figure 2 illustrates the resulting stiffness variations for the chosen values of a and b. The locations with x = 0 and 0.075 correspond to the left and right end of the OL, respectively. The user subroutine USDFLD in ABAQUS was used to implement the stiffness variation along OL in the finite element model.

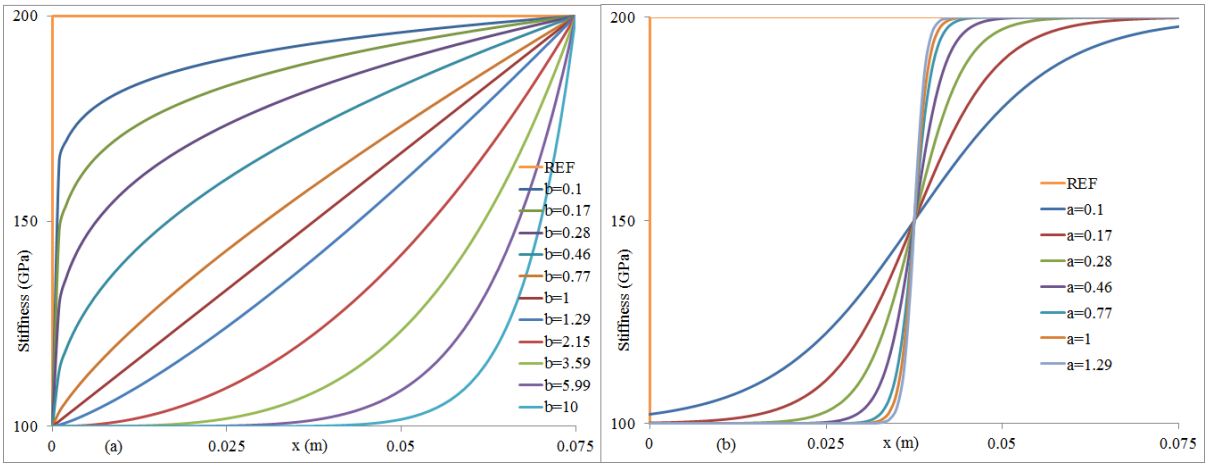

Figure 2. Variable stiffness functions (a) parabolic and (b) s-shaped functions.

The whole set of parabolic and s-shaped stiffness functions was additionally used to develop configurations where the stiffness $E(x)$ of the metal part varied between E_{min} and 200 GPa in the OL, with E_{min} varying from 0 to 90 GPa in steps of 10 GPa (see Tests 2-11 and 13-22, Table 1). These tests investigated the effect of stiffness variation range in the peak in-plane σ_{xy} shear stresses.

Finally, it was hypothesised that the stresses in the joint were critically dependent on the slope of the stiffness function at the ends of the OL of the joint. To investigate this hypothesis, linear functions were used at both ends of the overlap length for different distance from the ends L_S/t = 0.05, 0.1, 0.3, 0.5, 1, 2 (where L_S is the linear part of each variable stiffness function and t is the adherend's thickness, see Figure 3b), and different slopes. In the remaining central region of the overlap $OL_R = OL - 2L_S$, cubic and parabolic (b = 0.46 and b = 2.15) stiffness functions were applied to investigate the effect of the shape of the curve after a specific distance from the OL end (Ls/t) on the peak stresses at both ends of the OL. The parabolic curves in the OL_R were used to investigate the effect of abrupt changes in the stiffness curve to the peak stresses. Parabolic curves b = 0.46 and b = 2.15 gave an abrupt change in the stiffness curves close to the left and right ends of the bondline, respectively (see Figure 3). On the other hand, cubic curves in OL_R offered a smooth transition between the two linear parts of the curves. The effect in the peak stresses of four different slopes, in the linear part of these configurations, was also investigated (see Tests 23-94, Table 1).

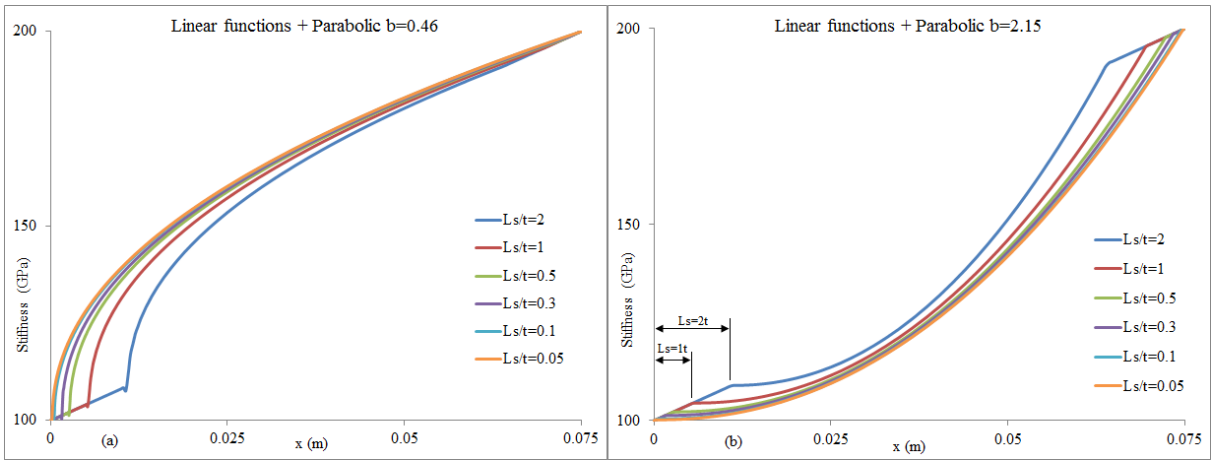

Figure 3. Variable stiffness functions (a) linear plus parabolic b = 0.46 and (b) linear plus parabolic b = 2.15.

Test	Stiffness variation in the metal part [GPa]	Stiffness function type	Slope of the linear part [GPa/mm]
REF	none (constant stiffness of 200)	-	-
1	100 to 200	parabolic (all b-values)	-
2	90 to 200	parabolic (all b-values)	-
3	80 to 200	parabolic (all b-values)	-
4	70 to 200	parabolic (all b-values)	-
5	60 to 200	parabolic (all b-values)	-
6	50 to 200	parabolic (all b-values)	-
7	40 to 200	parabolic (all b-values)	-
8	30 to 200	parabolic (all b-values)	-
9	20 to 200	parabolic (all b-values)	-
10	10 to 200	parabolic (all b-values)	-
11	0 to 200	parabolic (all b-values)	-
12	100 to 200	s-shaped (all a-values)	-
13-22	E_{min} to 200	s-shaped (all a-values)	-
23-28	100 to 200	linear (various L_S/t) and cubic	0.091
29-34	100 to 200	linear (various L_S/t) and cubic	0.363
35-40	100 to 200	linear (various L_S/t) and cubic	0.818
41-46	100 to 200	linear (various L_S/t) and cubic	4
47-52	100 to 200	linear (various L_S/t) and parabolic (b = 0.46)	0.091
53-58	100 to 200	linear (various L_S/t) and parabolic (b = 0.46)	0.363
59-64	100 to 200	linear (various L_S/t) and parabolic (b = 0.46)	0.818
65-70	100 to 200	linear (various L_S/t) and parabolic (b = 0.46)	4
71-76	100 to 200	linear (various L_S/t) and parabolic (b = 2.15)	0.091
77-82	100 to 200	linear (various L_S/t) and parabolic (b = 2.15)	0.363
83-88	100 to 200	linear (various L_S/t) and parabolic (b = 2.15)	0.818
89-94	100 to 200	linear (various L_S/t) and parabolic (b = 2.15)	4

Table 1. Configurations investigated.

3. Results and discussion

3.1. Effect of stiffness range variation

To investigate the effect of the proposed biomimetic solutions, stresses in the joints were obtained from the numerical results at the maximum force level. The REF SLJ configuration (i.e. no stiffness variation along the overlap length) was used to compare with the biomimetic SLJs. All the joints deformed in accordance with the well-known eccentric behavior of a SLJ in a way that led the adhesive layer to develop high in-plane shear stresses at the left and the right hand side edges of the bondline. Figure 4 shows the effect of the parabolic stiffness variation of Tests 1-11 in the steel on the peak in-plane σ_{xy} shear stresses developed at each end of the overlap region and for each different stiffness reduction. The diamond-shape and square-shape points refer to the peak stress at the left and right end of the bondline, respectively.

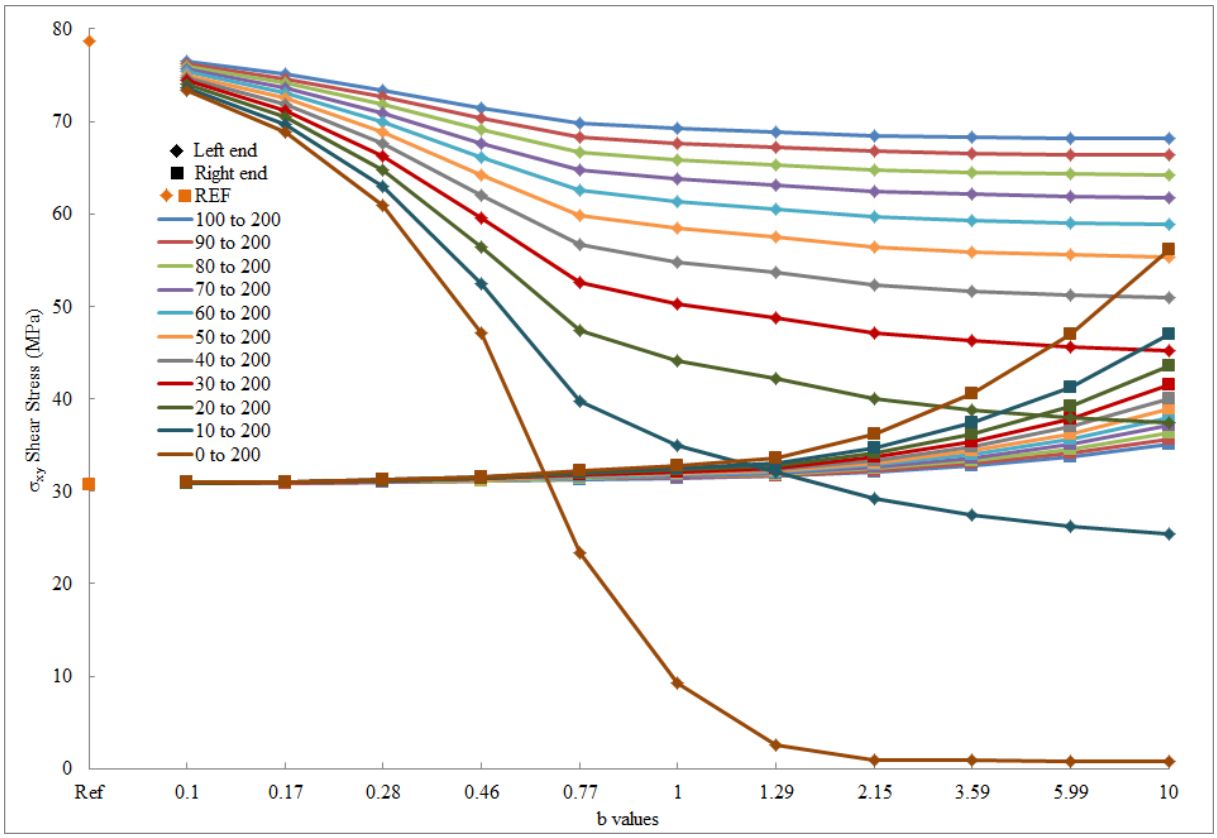

Figure 4. Effect of stiffness reduction on peak in-plane σ_{xy} shear stresses at both ends of the bondline, Tests 1-11 (parabolic functions).

As shown in Figure 4, the reference SLJ gives a non-uniform σ_{xy} shear stress distribution with peak values of 79 MPa (left end) and 31 MPa (right end). All the biomimetic SLJs reduced this asymmetry in stress distribution. In Tests 1-8 the failure of the joint is predicted to initiate at the left end of the bondline, as the stresses are higher for all different *b*-values. A nearly symmetrical σ_{xy} shear stress distribution was obtained in Test 10 (stiffness variation in metal part 10-200 GPa), when the parabolic b = 1.29 variable stiffness function was used. In this configuration, the peak σ_{xy} shear stresses were 32 and 33 MPa at the left and right ends, respectively, giving a reduction of 58% in the peak shear stress σ_{xy}. It is worth mentioning that Test 10 (with b = 1.29 or higher) will theoretically initiate failure at the right end of the joint.

Regarding the s-shape functions, the highest shear stress peak value was almost constant for each stiffness reduction (Tests 13-22) for the whole range of a-values (Figure 5). An almost symmetric σ_{xy} stress distribution was obtained in Test 21 (stiffness variation in metal part 10-200 GPa) for a = 0.17. In this configuration, the peak σ_{xy} shear stresses were 30 and 32 MPa at the left and right ends, respectively, and a 59% σ_{xy} shear stress reduction was obtained.

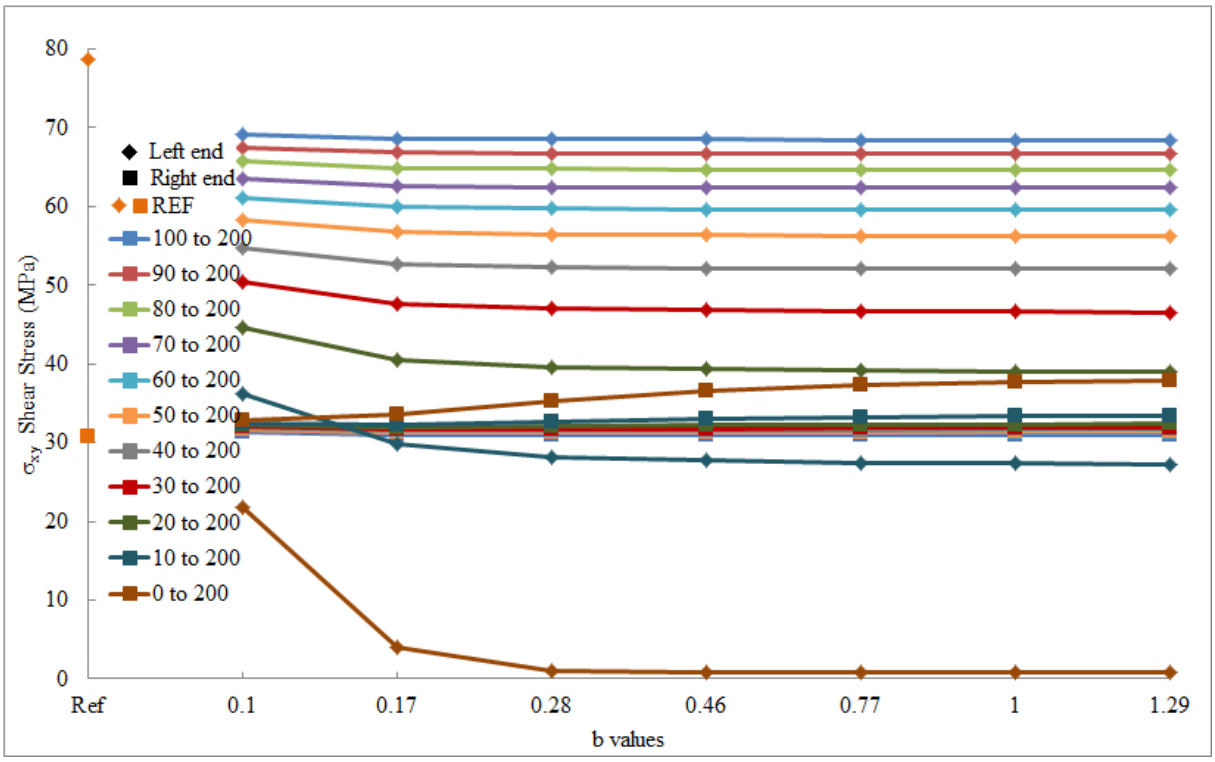

Figure 5. Effect of stiffness reduction on peak in-plane σ_{xy} shear stresses at both ends of the bondline, Tests 12-22 (s-shaped functions).

3.2. Effect of different linear curve lengths (L_S/t)

Figure 6 shows the effect of the linear length (L_S/t) of the stiffness variation on the peak in-plane σ_{xy} shear stresses developed at each end of the bondline, for a gradient of stiffness of 0.818 GPa/mm, stiffness variation between 100-200 GPa, and for different stiffness variations in OL_R (cubic, Tests 35-40; parabolic b = 0.46, Tests 59-64; parabolic b = 2.15, Tests 83-88). The effect of L_S/t on the peak stress variations of the remaining slopes are not given, since they share the same behavior with the 0.818 GPa/mm slope. A stress reduction of 10-12% was obtained, depending on the value of L_S/t and the shape of the stiffness curve applied in the central overlap region OL_R. As shown in Figure 6, the effect of L_S/t on the peak σ_{xy} shear stresses is negligible. A 2% stress reduction difference can be observed at the left end peak stresses and only when the parabolic b = 0.46 curve was applied in OL_R. This was expected because of the abrupt changes of the stiffness curve, close to the left end of the bondline, when the parabolic b = 0.46 curve was applied. Finally, it can be seen from Figure 6, that the shape of the curve in OL_R did not influence the peak σ_{xy} stresses, as the lines are almost identical.

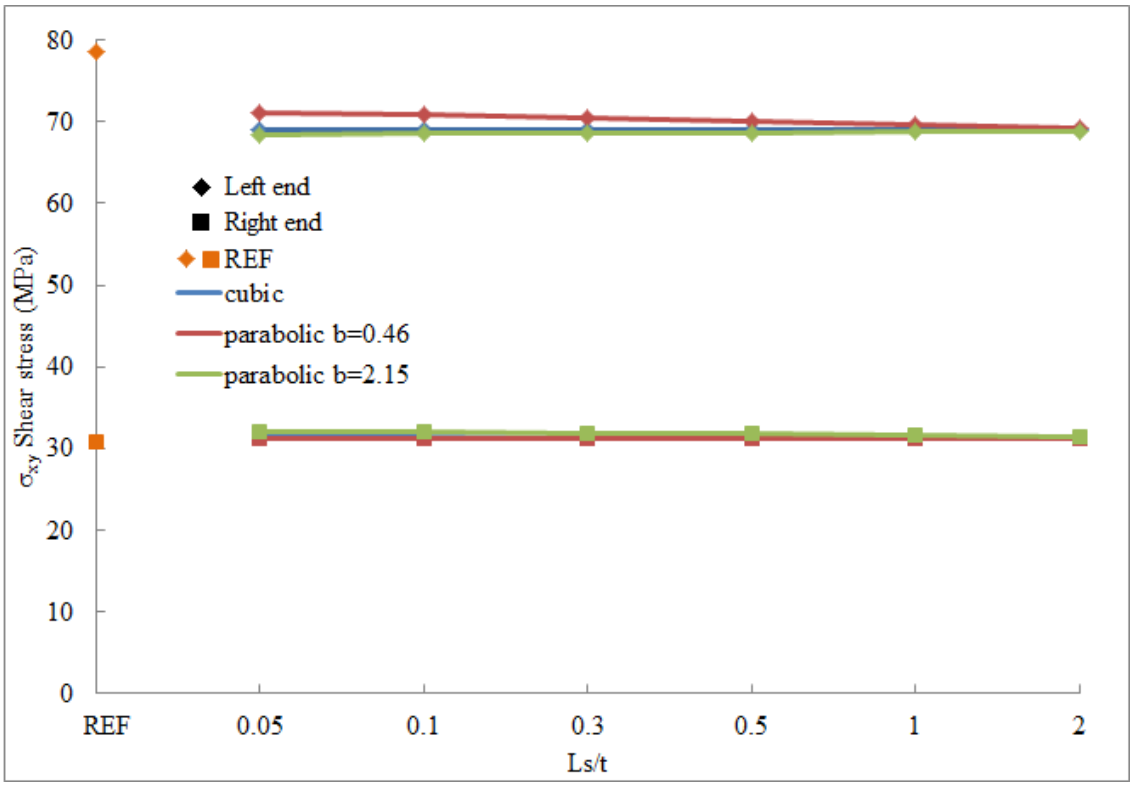

Figure 6. Effect of different linear stiffness change lengths (L_S/t) and shape of stiffness change in the central overlap region OL_R on the peak in-plane σ_{xy} and shear stresses at both ends of the bondline stiffness variation between 100-200 GPa, stiffness gradient in straight region = 0.818 GPa/mm . Tests 35-40 (cubic); Tests 59-64 (parabolic b = 0.46); and Tests 83-88 (parabolic b = 2.15).

3.3. Effect of slope of linear region of stiffness variation

Figure 7 shows the effect of the slope of the linear region of the stiffness variation on the peak in-plane σ_{xy} shear stresses developed at the left end of the bondline for stiffness range variation of 100-200 GPa. It was observed that, by increasing the slope in the linear part, and by using cubic curves in the OL_R (solid lines in Figure 7), the peak stresses were slightly increased. The stresses remain constant for all slopes in each of the cases when L_S/t = 0.05, 0.1 and a parabolic stiffness variation in the central region with b = 0.46 was used. This was expected because, for very small L_S/t, the stresses at the end of the bondline were influenced by the abrupt change of the variable stiffness curve. Generally, the different curves used to represent the stiffness variation in OL_R (cubic, parabolic b = 0.46 and b = 2.15) gave slightly different results for the peak stresses for the same slope (higher stress reduction difference 3%). However, for the case of L_S/t = 2, the three curves became almost identical throughout the slope variation. This result suggests that the peak stresses at the end of the bondline were not influenced by the shape of the variable stiffness function beyond a distance of $L_S = 2t$ from the bondline end.

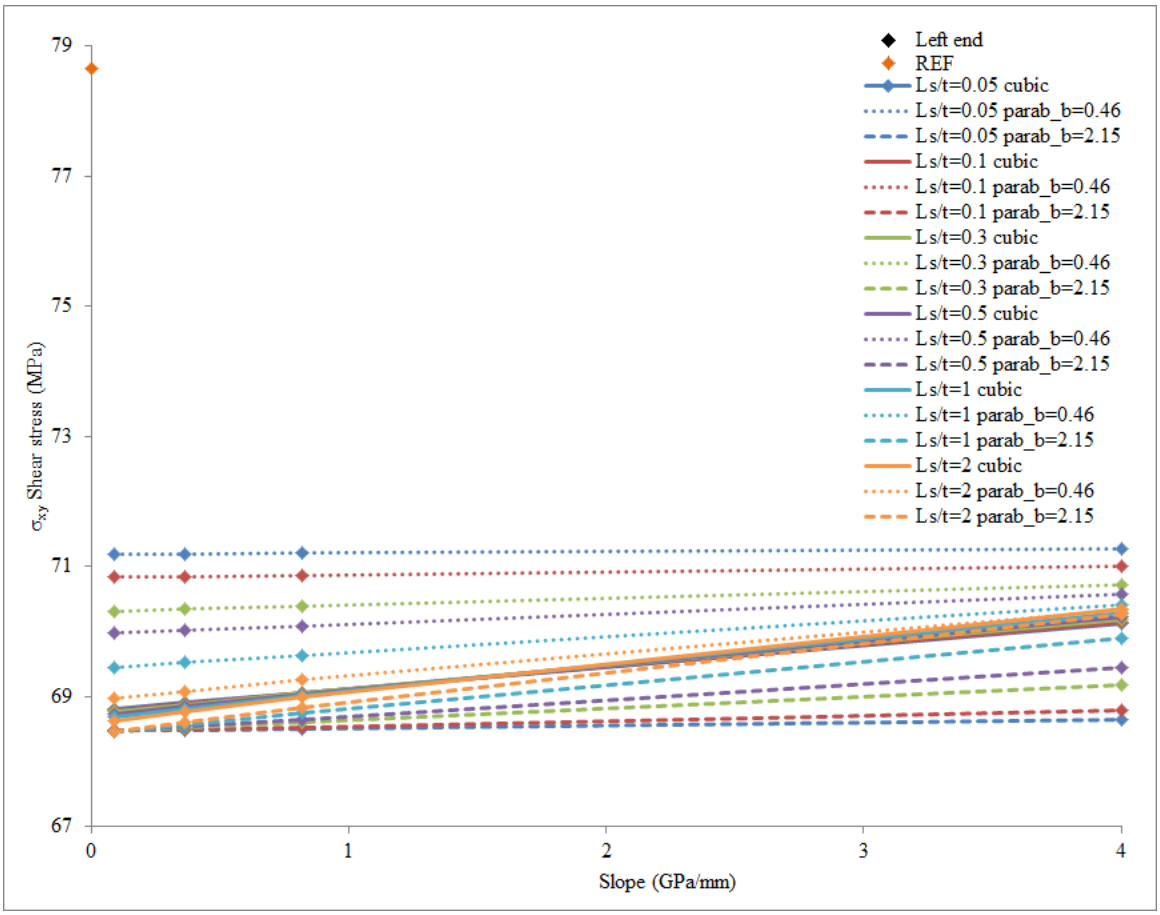

Figure 7. Effect of the linear curve slope on the peak in-plane σ_{xy} shear stresses at the left end of the bondline, Tests 23-94.

4. Conclusions

A finite element investigation of biomimetic-inspired SLJs between dissimilar adherends was presented. The proposed SLJs considered a transitional zone of stiffness in the joint site to reduce the material stiffness mismatch. All the proposed biomimetic solutions reduce the asymmetry of the stress distribution along the bondline. By increasing the stiffness reduction in the metal part of the joint, the stress reduction at the end of the bondline was increased with a maximum shear stress reduction of 59%. The rate of change of the stiffness with position at the ends of the bondline slightly influenced the peak stresses, giving a maximum change in stress of 3%.

Acknowledgements

The authors acknowledge the financial support provided by Engineering and Physical Sciences Research Council (EPSRC) and Dowty Propellers (part of GE Aviation).

References

[1] J. Cao and L. Grenestedt. Design and testing of joints for composite sandwich/steel hybrid ship hulls. *Composites: Part A*, 35:1091-1105, 2004.

[2] E. I. Avgoulas and M. P. F. Sutcliffe. Biomimetic-inspired joining of composite with metal structures: a survey of natural joints and application to single lap joints. In *SPIE Smart Structure/NDE: Bioinspiration, Biomimetics, and Bioreplication IV*, 2014.